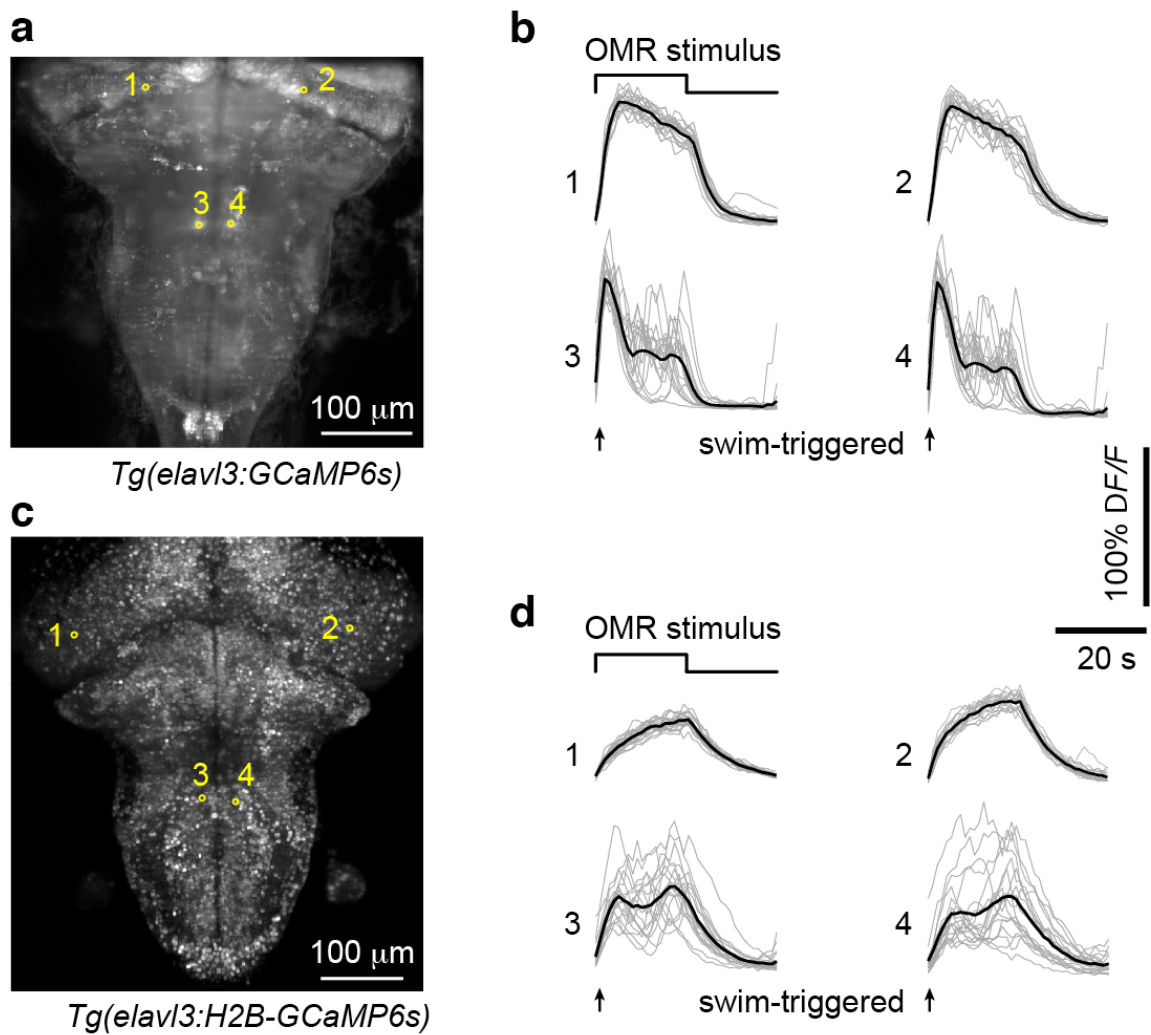


Supplementary Figure 1

The light-sheet microscope with behavior setup.

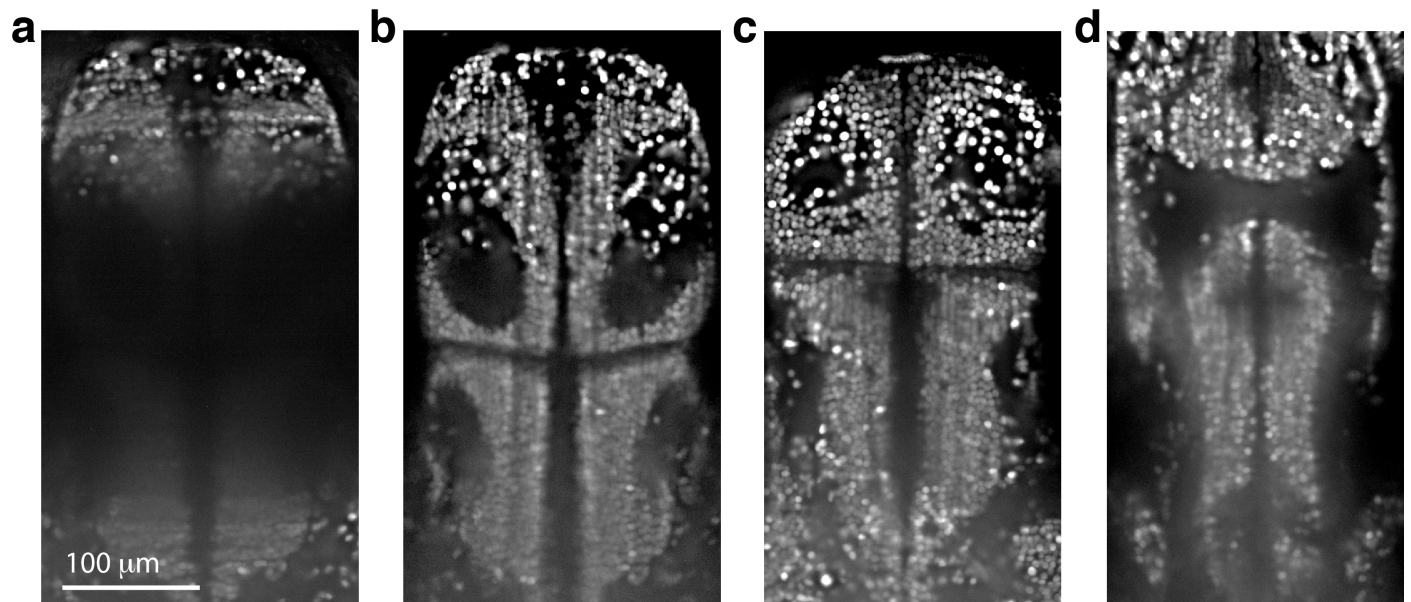
Lasers, control and data acquisition hardware are not shown.



Supplementary Figure 2

Neuronal activity reported by nuclear localized GCaMP6s.

(a) Locations of four example neurons in a 6 dpf *Tg(elavl3:GCaMP6s)* zebrafish, scanned with a light sheet microscope. (b) Calcium signals of the four neurons indicated in a during optomotor behavior. Traces 1,2 are triggered on stimulus onset; traces 3,4 on the onset of fictive swimming following stimulus onset. (c) Locations of four example neurons in a 6 dpf *Tg(elavl3:H2B-GCaMP6s)* zebrafish. (d) Calcium signals of these four neurons during the optomotor assay.



Supplementary Figure 3

Assessment of physical coverage and spatial resolution in *Tg(elavl3:H2B-GCaMP6s*) fish (nuclear-localized expression).

(a) Images of forebrain and midbrain acquired using only the lateral light sheet (215 micrometers from the top of the brain). (b) Same area, with both lateral and frontal light sheets. (Different fish from c,d.) (c) Example area between the eyes with mostly single-cell resolution (190 micrometers from the top), imaged with both light sheets. (d) Example area between the eyes including areas that lack single-cell resolution (175 micrometers from the top), imaged with both light sheets. Scale bar, 100 micrometers. Images have been normalized to the local brightness (where local brightness is computed by smoothing the raw image by a 2D Gaussian kernel with $\sigma = 5$ micrometers). See also Supplementary Movie 2 for the full volume.

Supplementary Note

Light-sheet functional imaging in fictively behaving zebrafish

Nikita Vladimirov, Yu Mu, Takashi Kawashima, Davis V Bennett, Chao-Tsung Yang, Loren L Looger, Philipp J Keller, Jeremy Freeman, Misha B Ahrens

Light-sheet microscope

We built a custom light-sheet microscope capable of imaging most of the brain of the larval zebrafish at cellular resolution, in which the animal was placed horizontally and intended motor output was recorded electrically and visual stimuli were presented from below (Suppl. Fig. 1). Most of the mechanical and optical components were identical to those used in a previously published system¹, with the following changes: The tip/tilt mirrors were replaced by pairs of galvanometer scanners, the PI Hera piezo stages were replaced by P-725.4CD piezo stages and the sample positioning system was replaced by a system of linear motors used to move the sample chamber after setting up the electrodes (Suppl. Table 1). The core electronics framework was revised to unify instrument control in a single computer workstation, thus replacing the combination of image acquisition workstation and separate real-time controller in the previous design. The microscope detection arm was rotated by 90 degrees to a vertical orientation, so that the zebrafish could be placed horizontally in its natural body position. We added an orthogonal illumination arm to scan the tissue between the eyes, which cannot be accessed using the lateral light sheet. Moreover, the lateral light sheet was dynamically switched off with microsecond precision when the laser entered the elliptical exclusion region covering each fish eye, thus minimizing the impact of illumination laser on visually driven fish behavior (Fig. 1b). The eye exclusion region was determined for each fish individually, using a white LED positioned below the chamber. The rapid (microsecond scale) switching of the laser power within the eye exclusion region was performed using the digital ‘enable’ shutter, which is built-in within the laser.

Detection arm

The detection arm consisted of a water-dipping detection objective (16x/0.8 NA, Nikon) mounted vertically on a piezo (P-725.4CD, Physik Instrumente), a tube lens (Nikon) and an sCMOS camera (Orca Flash 4.0, Hamamatsu). The z-position of the objective was controlled by the piezo using analog stepwise waveforms. Images were recorded using the sCMOS camera’s external trigger mode. The detection arm was furthermore equipped with a band-pass filter (525/50 nm) for separating GCaMP fluorescence light from laser light. An overview of all components is provided in Suppl. Table 1. At 16x magnification the sCMOS camera provides a field-of-view sufficient for imaging the entire brain of 5-7 dpf animals, at about 100 voxels per neuron.

Illumination arms

Each illumination arm consisted of an air illumination objective (4x/0.28 NA, Olympus) mounted horizontally on a piezo (P-725.4CD, Physik Instrumente), a tube lens (Olympus), an f-theta lens (Special Optics) and a pair of galvanometer scanners (Cambridge Technology). The scan mirrors and f-theta lens scanned the collimated laser beam (488 nm, SOLE-3, Omicron) laterally and along the z-axis. The z-position of the detection objective was matched to the z-location of the light sheet using the piezo in the

detection arm. For all experiments, we used a peak laser power, measured before the objective, in the range of 80-180 μ W for the lateral illumination arm, and 30-150 μ W for the front illumination arm.

Light-sheet properties and scan procedure

The laser beams were expanded by the scan/tube lens pair such that the weakly-focused lateral and frontal laser beams reached a central FWHM (full width at half maximum) thickness of about 4 micrometers in the center of the sample chamber. Light sheets were generated by fast scanning of these Gaussian laser beams. The lateral light sheet was generated by rapidly scanning the lateral laser beam over a distance of 900 micrometers along the rostro-caudal axis of the fish, while the frontal light-sheet was generated by rapidly scanning the frontal laser beam over a distance of 150 micrometers between the eyes, within the same z-plane. While executing both scans an image was acquired *via* the detection objective oriented at a right angle to both illumination objectives. Subsequently, the positions of the light sheets and the detection objective were moved by 5 micrometers in z, and the process was repeated. The imaging speed was limited by the camera readout speed and the resetting of the detection objective's piezo. We typically used exposure times of 6 ms (for 3 Hz volumetric rates) or 11 ms (for 2 Hz volumetric rates) per plane and a 100 ms objective reset time between volumes.

In the rolling shutter camera mode that was utilized, not all pixels on the camera chip are read out simultaneously; instead they are read out row-by-row in two sweeps propagating outward from the center line. In combination with the sweeping lasers, this means that different areas of a recorded image may represent neighboring anatomical planes, since in some areas, pixel readout may occur before laser excitation (and therefore reporting photons from the previously scanned plane), while in others, it may occur after laser excitation (reporting photons from the current scanned plane). These areas are delineated by straight lines, and a simple *post hoc* stitching procedure can be applied to recombine the anatomical planes from neighboring images. The need for this stitching can be circumvented by very quickly (e.g. in 0.5 ms) sweeping the laser beams across the plane before pixel readout begins. This method, however, requires higher peak laser power, because the same amount of excitation light has to be delivered to the plane in a shorter period of time.

Imaging and data logging

16-bit images were acquired with the Hamamatsu Orca Flash 4.0 sCMOS camera, providing about 40 images per brain volume at a volumetric imaging rate of 2-3 Hz (see above). Images were captured at 5 micrometer steps in z with a ~4-micrometer-thick light sheet (FWHM at the center of the sheet), such that each neuron in the imaged volume was covered, considering that a neuron is about 6 micrometers in diameter. The image data stream of ~320-475 MB/s provided by the Active Silicon FireBird frame grabber was saved to a RAID6 disk array in real-time using a binary image format. Hardware control and data logging were performed on a high-end workstation (Suppl. Table 1) using the custom-written LabVIEW software Zebrascope (Michael Coleman, Coleman Technologies). Experiments reported here typically lasted ~30 min, thus generating approximately 500 GB of imaging data per experiment. The microscope control software and the electrophysiology/stimulation software were synchronized using TTL pulses from the camera output trigger.

Image processing

All images were registered using translation registration in x and y relative to a reference stack (formed as an average of 100 stacks from the middle of experiment), by calculating cross-correlations between each image and the respective reference image (using MATLAB, MathWorks, Natick, MA). Motion artifacts mostly consisted of slow drift in the x-direction (along the specimen's body axis), on average 2-5 micrometers per experiment.

Data were analyzed using the *Thunder* library on the Janelia distributed computing cluster as detailed in a companion paper².

Nuclear-localized GCaMP

In an attempt to improve single-cell identifiability, and eliminate the mixing of neurite signals with somatic signals, we targeted GCaMP6s to the nucleus of imaged cells. This has previously been done through use of short nuclear-targeting peptides, resulting in decent nuclear retention³. To improve on this method, we fused GCaMP6s to human histone H2B in a similar fashion to H2B-GFP, which has been used routinely⁴. This should increase nuclear retention to ~100%, and further target fluorescence localization to sub-nuclear structures, both of which should improve single-cell identifiability. After establishment of a stable pan-neuronal *e/av/3* line, fish were characterized before use in experiments (Suppl. Fig. 2). Expression of pan-neuronal H2B-GCaMP6s did not appear to affect normal development, cellular division, or fish behavior (data not shown). GCaMP6s expression appeared completely limited to cellular nuclei (Suppl. Fig. 3), unlike cytoplasmic GCaMP6s, which is largely nuclear-excluded. H2B-GCaMP6s produced large fluorescence transients upon sensory stimulation, which showed slightly lower $\Delta F/F$ and slower rise and decay kinetics than cytoplasmic GCaMP6s, unsurprisingly (Suppl. Fig. 2b,d) – variants using faster calcium indicators, e.g. GCaMP6f⁵, will likely have more rapid rise and decay kinetics. The signal to noise ratio from H2B-GCaMP6s was high, allowing detection of similar activity patterns as cytoplasmic GCaMP6s.

Single-cell resolution

Compared to previous work¹ the current setup has an additional light-sheet from the front, revealing a larger fraction of cells at single-cell resolution (Suppl. Fig. 3a,b; Suppl. Video 2). Since single-neuron resolution generated by the lateral light sheet has been previously assessed¹, here we assessed single-neuron coverage generated by the frontal light sheet in areas inaccessible to the lateral light sheet (Suppl. Fig. 3a). The volume between the eyes (most of the forebrain and parts of the midbrain) was evaluated, by eye, and areas were manually annotated to either have anatomical single-cell resolution (as in Suppl. Fig. 3c) or to have lower than single-cell resolution (as in areas of Suppl. Fig. 3d). This yielded an estimate of ~81% of the volume to be covered at single-cell resolution. This is here assessed using a nuclear localized calcium indicator, but we expect comparable results for cytoplasmic calcium indicators. Note that segmentation based on neuronal activity will increase the effective degree of single-cell resolution because the signal fluctuations can be used in addition to anatomy to segment cells.

Fish mounting

Fish were mounted on a custom-made holder that provides mechanical support for the fish's head and body, and constrains lateral drift with walls on both sides of the animal (Suppl. Fig. 1), while leaving the fish's tail unobstructed for electrode access. These sample holders were cut from acrylic using a laser cutter, or 3D-printed (STL model available upon request). For the purpose of specimen illumination with laser light, the sample chamber has transparent windows made of cover slips. The chamber walls are black in order to minimize internal reflection of the laser beam. For sample mounting, the chamber was filled with 2% low-melting point agarose (Sigma-Aldrich Inc.) and the paralyzed fish was quickly placed on the sample holder. Once the agarose was fully gelled, system water was added and agarose in the tail and head region was removed with a scalpel. This mounting method ensures optical and electrical exposure of all specimen regions relevant in our imaging experiments. The chamber is mounted on a custom-made stage that is positioned in three dimensions by using three motorized translation stages (Suppl. Table 1 and Suppl. Fig. 1).

Behavioral setup and experiments

All experiments were conducted according to protocols approved by the Institutional Animal Care and Use Committee of the Howard Hughes Medical Institute, Janelia Farm Research Campus. Larval zebrafish were paralyzed by brief immersion into 1 mg/ml alpha-bungarotoxin solution (Invitrogen). Once paralyzed, the fish were embedded using 2% low-melting point agarose (Sigma-Aldrich Inc.) in a custom-made chamber as described above. After transporting the chamber to the experimental apparatus, electrical recordings from the ventral root of the spinal cord, or motor neuron axons, were made according to previously described techniques^{6,7}. Briefly, extracellular recordings were made with fire-polished glass pipettes with tip diameter approximately 40 micrometers using an Axon Multiclamp 700B amplifier in current clamp. Electrodes were advanced using manual micromanipulators (Siskiyou) until they touched the dorsal part of the intact tail, after which gentle suction was applied to seal them to the tissue and record signals from the ventral root (intended motor output of the paralyzed fish). Signals were sampled at 6 kHz, and band-pass filtered with a low-pass cutoff at 1.4 kHz and a high-pass cutoff at 100 Hz or 300 Hz. To identify swim bouts, signals were further processed by taking the local standard deviation in a sliding 10 ms window. Signals were recorded and visual stimuli presented using custom software written in C# (Microsoft).

Visual stimulus delivery

The fish holder was mounted on the transparent acrylic bottom section of the chamber, which simplified the process of removing agarose surrounding the animal. A diffusive plastic screen was attached to the bottom of the chamber from the outside, to allow image projections from below using a miniature projector producing red monochromatic images.

Optomotor response

A red/black grating of spatial period ~1.2 cm moving forward, from tail to head, at a speed of 0.24 cm/s was presented to the fish, alternating between periods of static stimulus and motion. During visual motion, vigorous fictive swimming was observed, while during no motion, the fish swam little. The OMR experiments were open-loop, so fictive swimming of fish did not affect the stimulus motion. Duration of

experiment was typically 10 min, with 15 trials of OMR: 20 s of static stimulus followed by 20 s of moving stimulus. When evaluating the effect of imaging on behavior (Fig. 1c), the fish were given 10 minutes at the start of imaging to adapt to the presence of the light sheet, although most fish did not require this.

Motor adaptation

Motor adaptation⁸ experiments were performed as described elsewhere¹. Briefly, the same grating as described above for OMR was slowly drifting forwards, from tail to head, at a speed of 0.24 cm/s, simulating backwards motion of the fish along a one dimensional virtual track. Fictive swim bouts were translated into forward motion along the virtual track according to: $velocity = gain \times motor\ output$. The feedback gain was alternated every 20 s between low and high (difference by a factor of 3), making fish swim more (low gain) or less intensively (high gain). Like in the OMR, fish were given 10 minutes to adapt to the light sheet, but most did not require this.

Behavioral quantification

To capture the magnitude of stimulus-induced swimming during the optomotor response, we defined an optomotor index as follows. First, one of two electrophysiological channels were selected for analysis from each recording by hand, based on signal-to-noise ratio and signal stationarity. Second, the time course of swimming strength was averaged across repeated presentations, separately for the two laser conditions. Third, the minimum of each time course was subtracted from it, to ensure responses were positive. Fourth, responses were averaged within two 8 s windows, one in the middle of the period of no stimulation, and the other immediately after stimulus presentation (to capture the transient response to the stimulus). Small changes to the timing of this window did not qualitatively change the result. Finally, for each fish and condition (laser or no laser), an index was computed as the difference in swimming strength during and before the stimulus, divided by the sum. For statistical analysis, to avoid any parametric assumptions, these indices were compared to 0 using a two-sided sign test, as well as compared between laser conditions (across fish) with a two-sided paired sign test. Test results were qualitatively similar when using t-tests.

To capture the effect of gain changes on swimming, we defined a gain adaptation index. The preprocessing was the same as for the optomotor index, except that responses were averaged within two 8 s windows each in the middle of the high-gain and low-gain periods, respectively. The index was computed as the ratio of swimming strength during high gain and during low gain, which is more appropriate than a difference because the feedback signal for closed-loop swimming is a multiplicative factor of swimming strength. For statistical analyses, to avoid any parametric assumptions, these indices were compared to 1 using a two-sided sign test, as well as compared between laser conditions (across fish) with a two-sided paired sign test. Test results were qualitatively similar when using t-tests.

Two of the tested fish were discarded from the analysis because of substantial drift in the electrophysiological recording.

Transgenesis

Zebrafish lines generated for this study are *Tg(elavl3:GCaMP6s)*^{if4} and a nuclear-localized GCaMP6s line *Tg(elavl3:H2B-GCaMP6s)*^{if5}, both in the *nacre* background. The fish lines were generated using the Tol2 transposon system⁹. In the case of the nuclear-localized indicator, *GCaMP6s*⁵ was fused with the human histone *H2B* gene⁴ at the 5'-end to restrict its expression to the nucleus. The *GCaMP6s* gene and the *H2B-GCaMP6s* fusion gene were sub-cloned into a Tol2 vector that contained the zebrafish *elavl3* promoter. The transgene construct and transposase mRNA were injected into 1-4 cell-stage embryos and the transgenic lines were isolated by the high expression of bright green fluorescence in the central nervous system in the next generation. Embryos were reared according to standard protocol at 28.5°C, and experiments were performed on animals 5-8 dpf at room temperature. Fish lines are available upon request.

1. Ahrens, M. B., Orger, M. B., Robson, D. N., Li, J. M. & Keller, P. J. Whole-brain functional imaging at cellular resolution using light-sheet microscopy. *Nature Methods* **10**, 413–420 (2013).
2. Freeman, J. et al. Mapping brain activity at scale with cluster computing. *Nature Methods* doi:10.1038/nmeth.3040 (27 July 2014).
3. Schrödel, T., Prevedel, R., Aumayr, K., Zimmer, M. & Vaziri, A. Brain-wide 3D imaging of neuronal activity in *Caenorhabditis elegans* with sculpted light. *Nature Methods* **10**, 1013–1020 (2013).
4. Kanda, T., Sullivan, K. F. & Wahl, G. M. Histone-GFP fusion protein enables sensitive analysis of chromosome dynamics in living mammalian cells. *Curr Biol* **8**, 377–385 (1998).
5. Chen, T.-W. et al. Ultrasensitive fluorescent proteins for imaging neuronal activity. *Nature* **499**, 295–300 (2013).
6. Masino, M. A. & Fetcho, J. R. Fictive swimming motor patterns in wild type and mutant larval zebrafish. *J Neurophysiol* **93**, 3177–3188 (2005).
7. Ahrens, M. B. et al. Brain-wide neuronal dynamics during motor adaptation in zebrafish. *Nature* **485**, 471–477 (2012).
8. Portugues, R. & Engert, F. Adaptive locomotor behavior in larval zebrafish. *Front Syst Neurosci* **5**, 72 (2011).
9. Urasaki, A., Morvan, G. & Kawakami, K. Functional dissection of the Tol2 transposable element identified the minimal cis-sequence and a highly repetitive sequence in the subterminal region essential for transposition. *Genetics* **174**, 639–649 (2006).

Supplementary Table 1. List of components of the experimental setup.

Module	Component	Product	Manufacturer
Lasers	SOLE-3 module	Solid-state, PhoXX 488 nm DPSS lasers 561, 594 nm	Omicron
Illumination module (2 modules)	Set of two orthogonal galvanometric mirrors	Model 6215H Optical Scanner	Cambridge Technology
	Driver board for two galvanometric mirrors	MicroMax 673XX	Cambridge Technology
	F-theta lens	66-S80-30T-488-1100nm custom lens	Special Optics
	Tube lens	U-TLU-1-2	Olympus
	Piezo objective positioner	P-725.4CD piezo stage E665 piezo amplifier	Physik Instrumente
	Illumination objective	XLFLUOR 4x, NA 0.28	Olympus
	Filter wheel	96A351 filter wheel MAC6000 DC servo controller	Ludl
		NDQ neutral density filters	Melles Griot
Detection module	Detection objective	CFI LWD 16xW, NA 0.8 water-dipping objective	Nikon
	Piezo objective positioner	P-725.4CD piezo stage E665 piezo amplifier	Physik Instrumente
	Detection filter wheel	96A354 filter wheel MAC6000 DC servo controller	Ludl
		525/50 nm BrightLine band-pass filter (diameter 32 mm)	Semrock
	Tube lens module	CFI second objective lens unit, f=20 mm	Nikon
	Camera	Orca Flash 4.0 V. 2 (C11440-22C)	Hamamatsu
Specimen positioning system	Motorized stages (2 translation and 1 vertical)	M-521.DD M-511.DD M-501.1PD C-884 Four Axis Motion Controller	Physik Instrumente
Real-time electronics	Computer (PCI) control of PXI boards	PXI-8360 MXI-Express	National Instruments
	I/O interface boards (3 units)	PXI-6733 high-speed analog output board	National Instruments
	BNC connector boxes	BNC-2110 shielded connector block	National Instruments
	Serial interface	PXI-8432/2	National Instruments

	board		
	PXI chassis	NI PXI-1042Q	National Instruments
Control software	LabVIEW 2012 64-bit code	Zebrascope	Coleman Technologies
	LabVIEW functions and device drivers	Vision Development module 2012 NI-RIO NI-Motion NI-VISA NI-Serial	National Instruments
	Visual stimulus presentation and behavior recording	C# programs ZebraStim, BehaveAndScan	custom-made
Workstation and Servers	Imaging acquisition workstation	SX6750 Workstation Base Platform	Colfax
		2x Intel Xeon E5-2687W 3.1GHz CPUs	Intel
		16x DIMM 16384 MB DDR-3 RAM modules	unspecified
		FireBird Camera Link Deca frame grabber	Active Silicon
		Nvidia Quadro 2000D graphics card	Nvidia
		(2x) Intel 520 Series SSD (SATA) 480GB 6Gbps hard drives (RAID1)	Intel
		(14x) SAS 900GB 6Gbps hard drives (RAID6)	Western Digital
		Intel RS2WG160 SAS RAID controller	Intel
		Intel X520-SR1 PCI-E x 8 10Gb optic fiber network adapter	Intel
		Windows 7 Ultimate SP1	Microsoft
	Electrophysiology and stimulus presentation workstation	Intel Core i7-3820 Sandy Bridge-E 3.6GHz CPU	Intel
		ASUS P9X79 PRO motherboard	ASUS
		Corsair Vengeance 64GB (8 x 8GB) DDR-3 RAM	Corsair
		NI PCIe-6363 X Series Data Acquisition board	National Instruments
		BNC-2110 shielded connector block	National Instruments
		AAXA M2 miniprojector	AAXA Technologies
Electrophysiology	Microelectrode Amplifier	Axon Multiclamp 700B	Molecular Devices
	Manual micromanipulators	MX130	Siskiyou